

Least Squares Shadowing sensitivity analysis of chaotic limit cycle oscillations

Qiqi Wang^{a,*}, Rui Hu^a, Patrick Blonigan^a

^a*Aeronautics and Astronautics, MIT, 77 Mass Ave, Cambridge, MA 02139, USA*

Abstract

The adjoint method, among other sensitivity analysis methods, can fail in chaotic dynamical systems. The result from these methods can be too large, often by orders of magnitude, when the result is the derivative of a long time averaged quantity. This failure is known to be caused by ill-conditioned initial value problems. This paper overcomes this failure by replacing the initial value problem with the well-conditioned “least squares shadowing (LSS) problem”. The LSS problem is then linearized in our sensitivity analysis algorithm, which computes a derivative that converges to the derivative of the infinitely long time average. We demonstrate our algorithm in several dynamical systems exhibiting both periodic and chaotic oscillations.

Keywords: Sensitivity analysis, linear response, adjoint equation, unsteady adjoint, chaos, statistics, climate, least squares shadowing

1. Introduction

As more scientists and engineers use computer simulations, some begins to harness the versatile power of sensitivity analysis. It helps them engineer products [1, 2], control processes and systems [3, 4], solve inverse problems [5], estimate simulation errors [6, 7, 8, 9], assimilate measurement data [10, 11] and quantify uncertainties [12].

Sensitivity analysis computes the derivative of outputs to inputs of a simulation. Conventional methods, including the tangent and the adjoint method, are introduced in Section 2. These methods, however, fails when the dynamical system is chaotic and the outputs are long time averaged quantities. They compute derivatives that are orders of magnitude too large, and that grow exponentially larger as the simulation runs longer. What causes this failure is the “butterfly effect” – sensitivity of chaotic initial value problems. This diagnosis is first published by Lea et al [13], and explained in Section 3.

*Corresponding author.

Email addresses: qiqi@mit.edu (Qiqi Wang), hurui@mit.edu (Rui Hu), blonigan@mit.edu (Patrick Blonigan)

Many researchers have become interested in overcoming this failure, a challenge in both dynamical systems and numerical methods. They have recently developed a few methods for computing *useful* derivatives of long time averaged outputs in chaotic dynamical systems. Lea et al pioneered the ensemble adjoint method [13, 14], which applies the adjoint method to many random trajectories, then averages the computed derivatives. Nevertheless, they need impractically many trajectories, making the method costly even for small dynamical systems such as the Lorenz system. Thuburn introduced an approach that solves the adjoint of the Fokker-Planck equation, which governs a probability distribution in the phase space [15]. However, this approach assumes the probability distribution to be smooth, a property often achieved by adding dissipation to the Fokker Planck equation, causing error in the result.

In addition, researchers have adopted the Fluctuation-Dissipation Theorem for sensitivity analysis [16]. This approach has several variants. Different variants, however, have different limitations. Some assume the dynamical system to have an equilibrium distribution similar to the Gaussian distribution, an assumption often violated in dissipative dynamical systems. Other variants non-parametrically estimate the equilibrium distribution [17], but add artificial noise to the dynamical system to ensure its smoothness. The first author recently used Lyapunov eigenvector decomposition for sensitivity analysis [18]. However, this decomposition requires high computational cost when the dynamical system has many positive Lyapunov exponents. Despite these new methods, nobody has applied sensitivity analysis to long time averaged outputs in turbulent flows, or other large, dissipative and chaotic systems.

This paper presents the *Least Squares Shadowing method*, a new method for computing derivatives of long time averaged outputs in chaos. The method linearizes the *least squares shadowing problem*, a constrained least squares problem defined in Section 4. It then solves the linearized problem with a numerical method described in Section 5. Demonstrated with three applications in Sections 6, 7 and 8, the method is concluded in Section 9 to be potentially useful in large chaotic dynamical systems.

2. Conventional method for sensitivity analysis

In sensitivity analysis, an output J depends on an input s via a simulation, which solves an ordinary differential equation

$$\frac{du}{dt} = f(u, s) \tag{1}$$

starting from an initial condition

$$u|_{t=0} = u_0(s), \tag{2}$$

where the input s can represent control variables, design variables, and uncertain parameters. This initial value problem (1-2) determines a solution $u_{iv}(t; s)$ that depends on time and the input.

An output $J(u, s)$ is a function of the solution and the input. It can also be viewed as a function of time and the input by substituting the solution $u_{iv}(t; s)$. The time averaged output,

$$\bar{J}_{iv}^{(T)}(s) := \frac{1}{T} \int_0^T J(u_{iv}(t; s), s) dt, \quad (3)$$

then depends only on the input s . Its derivative to s can be computed by the conventional tangent method of sensitivity analysis [19].

The conventional tangent method first solves the linearized governing equation, also known as the *tangent equation*,

$$\frac{dv}{dt} = \frac{\partial f(u_{iv}, s)}{\partial u} v + \frac{\partial f(u_{iv}, s)}{\partial s} \quad (4)$$

with the linearized initial condition

$$v|_{t=0} = \frac{du_0}{ds}. \quad (5)$$

The solution $v_{iv}(t; s)$ indicates how a small change in s alters the solution to the initial value problem $u_{iv}(t; s)$:

$$v_{iv}(t; s) = \frac{\partial u_{iv}(t; s)}{\partial s} \quad (6)$$

This solution is then used to compute the derivative of $\bar{J}_{iv}^{(T)}(s)$:

$$\frac{d\bar{J}_{iv}^{(T)}}{ds} = \frac{1}{T} \int_0^T \left(\frac{\partial J(u_{iv}, s)}{\partial u} v_{iv} + \frac{dJ(u_{iv}, s)}{ds} \right) dt \quad (7)$$

This method can be transformed into the conventional adjoint method [19], which computes the derivative of one objective function to many inputs simultaneously. This advantage makes the adjoint method popular in optimal control, inverse problems and data assimilation applications.

3. Failure of the conventional method for time averaged outputs in chaos

The conventional method fails when the simulation (1) is chaotic, and the output (3) is averaged over a long time T . A chaotic dynamical system is sensitive to its initial condition, causing the solution to the linearized initial value problem (4) to grow at a rate of $e^{\lambda t}$, where $\lambda > 0$ is the maximal Lyapunov exponent of the dynamical system. This exponential growth makes $v_{iv}(t; s)$ large unless t is small. When substituted into Equation (7), we expect a large $\frac{d\bar{J}_{iv}^{(T)}}{ds}$ unless T is small.

The value of $\frac{d\bar{J}_{iv}^{(T)}}{ds}$ can exceed 10^{100} time of what scientists had expected. Lea et al. [13] documented this in the Lorenz system, which models heat convection from a warm horizontal surface to a cooler one placed above it. Their

temperature difference, described by the Rayleigh number, affects how fast the heat convects; it is therefore chosen by Lea et al. as the input s . The heat convection rate is chosen as the output J ; its time average should increase with s at a ratio of about 1.¹

Lea et al. considered a range of input s and several values of the averaging length T . At each s and T , they simulated the Lorenz system and computed $\overline{J}_{iv}^{(T)}(s)$. They then computed the derivative $\frac{d\overline{J}_{iv}^{(T)}}{ds}$ using the conventional adjoint sensitivity analysis method. When T is large, they found the derivative of $d\overline{J}_{iv}^{(T)}$ orders of magnitude larger than its expected slope of about 1. By repeating Lea et al.’s procedure, we found that the astronomical values of $\frac{d\overline{J}_{iv}^{(T)}}{ds}$, plotted in Figure 1, are insensitive to how Equations (1-7) are discretized.

The computed derivative $\frac{d\overline{J}_{iv}^{(T)}}{ds}$ is too large to be useful. The derivative is useful in approximating the slope of the function, $\frac{\overline{J}_{iv}^{(T)}(s+\delta s) - \overline{J}_{iv}^{(T)}(s)}{\delta s}$. The better it approximates this slope, and over a larger interval size δs , the more useful it is. If the derivative is as large as 10^{50} , the function must have a correspondingly steep slope when plotted against s , but only so monotonically over intervals smaller than 10^{-50} . The derivative can approximate the slope of the function well only within these impractically tiny intervals – computers cannot even represent an interval of $[1, 1 + 10^{-16}]$ in double precision. For approximating the slope of the function over a practical interval $[s, s + \delta s]$, the derivative is useless.

This failure happens not only to the Lorenz system, but to other chaotic dynamical systems such as chaotic fluid flows [20]. It is caused by the sensitivity to chaos. Popularly known as the “butterfly effect”, this sensitivity makes the finite time average $\overline{J}_{iv}^{(T)}$ ill-behaved, its derivative with respect to s fluctuating wildly. A small change in s almost always causes a large change in the solution u_{iv} , thus a large change in the tangent solution v_{iv} , and thus a large change in the derivative $\frac{d\overline{J}_{iv}^{(T)}}{ds}$. As s increases to $s + \delta s$, the derivative can vary over a wide range of positive and negative values. These derivative values, by the fundamental theorem of calculus, must average to the slope of the function

$$\text{slope} := \frac{\overline{J}_{iv}^{(T)}(s + \delta s) - \overline{J}_{iv}^{(T)}(s)}{\delta s} = \frac{1}{\delta s} \int_s^{s+\delta s} \frac{d\overline{J}_{iv}^{(T)}}{ds} ds', \quad (8)$$

but because the derivative fluctuates rapidly and wildly between extreme values of either sign, at almost any point within $[s, s + \delta s]$, the derivative is much larger in magnitude than the slope of the function over $[s, s + \delta s]$.

How sensitive a solution u is to its input s can be quantified by the *condition number*, defined as $\|du/ds\|$. We call a problem ill-conditioned if it has a large

¹In Lea et al.’s original paper, the Rayleigh number is denoted as ρ and the convective heat transfer rate is denoted as z . These notations are conventional in Lorenz system literature. But in this paper, we denote the Rayleigh number as s and the heat transfer rate as J , so that we are consistent with the general notation of input and output.

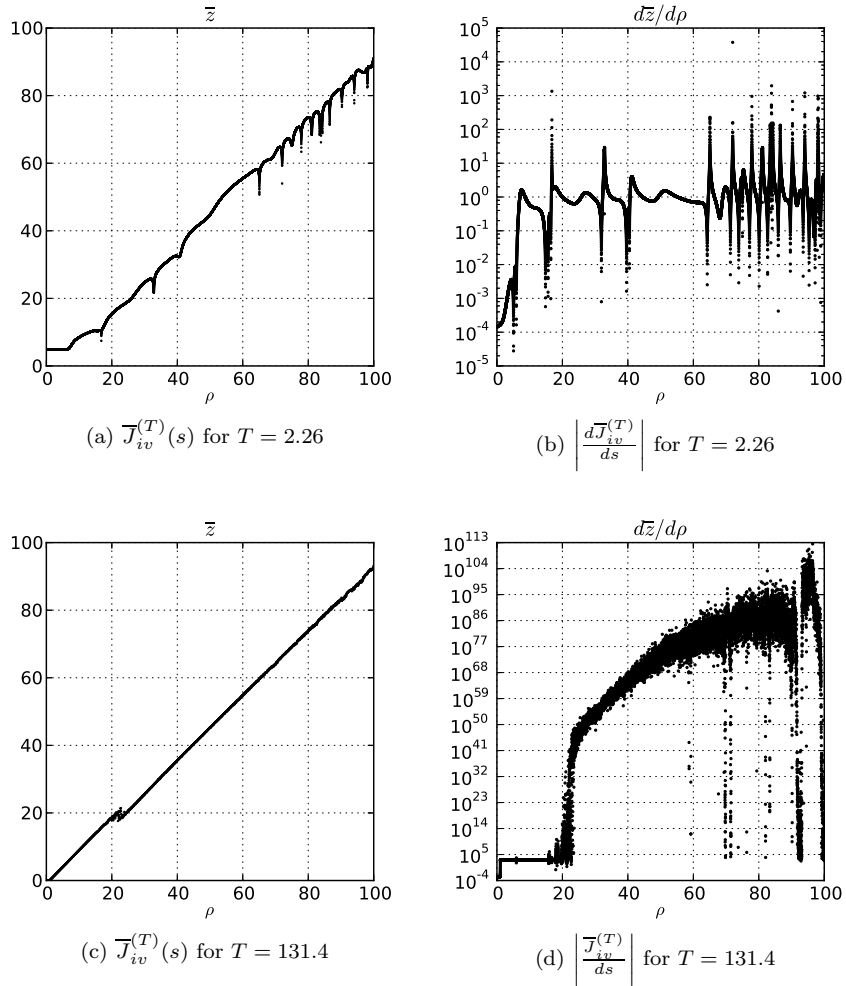


Figure 1: Plots created following the procedure in Lea et al[13] (permission granted). Left: time averaged output $\bar{J}_{iv}^{(T)}(s)$ plotted against the input s . Right: the derivative of the time averaged output with respect to s . Note the order of magnitude of the y -axes.

condition number, or well-conditioned if it has a small one. A chaotic initial value problem has a condition number on the order of $e^{\lambda T}$, where λ is the maximal Lyapunov exponent. Even moderately long simulations can be ill-conditioned, causing sensitivity analysis to fail. To overcome this failure, we must substitute the initial value problem with a well-conditioned one.

4. Sensitivity analysis via Least Squares Shadowing

4.1. The nonlinear Least Squares Shadowing (LSS) problem

The initial condition of a simulation can be relaxed if the following assumptions hold:

1. **We are interested in infinite time averaged outputs.** When scientists and engineers compute a long time averaged output, they often intend to approximate the limit

$$\overline{J}^{(\infty)}(s) := \lim_{T \rightarrow \infty} \frac{1}{T} \int_0^T J(u(t; s), s) dt. \quad (9)$$

We assume that these infinite time averaged outputs, and functions thereof, are the only outputs of interest.

2. **The dynamical system is *ergodic*.** An ergodic dynamical system behaves the same over long time, independent of its initial condition. Specifically, the initial condition does not affect an infinite time averaged outputs defined above.

Under these two assumptions, we can approximate the outputs using a long solution of the governing equation, regardless of where the solution starts. We replace initial condition with a criterion that makes the problem better-conditioned. Among all trajectories that satisfy the governing equation, we chose one that is closest to a pre-specified reference trajectory u_r in the following metric:

$$\begin{aligned} & \underset{\tau, u}{\text{minimize}} \frac{1}{T} \int_0^T \left(\left\| u(\tau(t)) - u_r(t) \right\|^2 + \alpha^2 \left(\frac{d\tau}{dt} - 1 \right)^2 \right) dt, \\ & \text{such that} \quad \frac{du}{dt} = f(u, s). \end{aligned} \quad (10)$$

We choose the reference trajectory $u_r(t)$ to be a solution to the governing equation at a different s , set the constant α so that the two terms in the integral have similar magnitude, then minimize this metric among all trajectories $u(t)$ and all monotonically increasing time transformations $\tau(t)$.

We call this constrained minimization problem (10) the Least Squares Shadowing (LSS) problem. We denote its solution as $u_{lss}^{(T)}(t; s)$ and $\tau_{lss}^{(T)}(t; s)$. They are a solution of the governing equation and a time transformation that makes this solution close to u_r . Because $u_{lss}^{(T)}(t; s)$ satisfies the governing equation, we use it to approximate

$$\overline{J}^{(\infty)}(s) \approx \overline{J}_{lss}^{(T)}(s) := \frac{1}{\tau(T) - \tau(0)} \int_{\tau(0)}^{\tau(T)} J(u_{lss}^{(T)}(t; s), s) dt. \quad (11)$$

with sufficiently large T .

4.2. Well-conditioning of the Least Squares Shadowing (LSS) problem

An initial value problem of chaos is ill-conditioned, causing failure to conventional sensitivity analysis methods, a failure we now overcome by switching to the LSS problem, a well-conditioned problem whose solution is less sensitive to perturbations in the parameter value, and whose long time averages have useful derivatives.

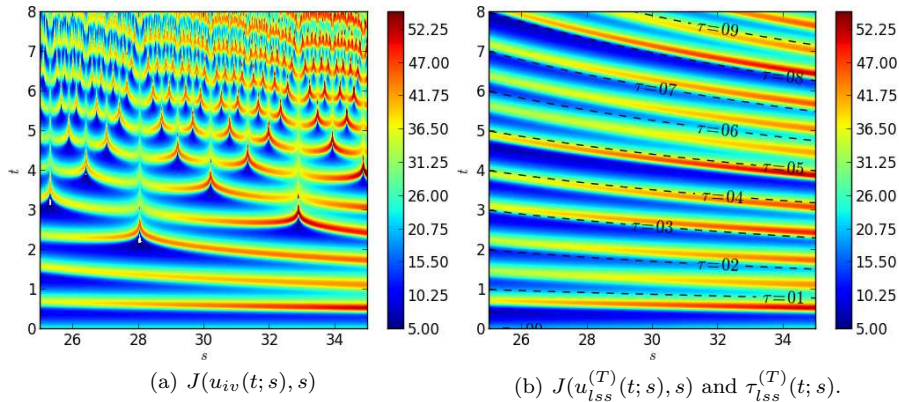


Figure 2: Time dependent rate of heat transfer in the Lorenz system with varying Rayleigh number s . This output is computed by solving initial value problems in the left plot, and by solving LSS problems in the right plot. Each vertical slice represents the time dependent output at an s value.

Figure 2 visualizes how sensitive the initial value problem is, whereas how robust the LSS problem is². The initial value problem produces solutions that grows more sensitive to the input s as time advances. Its condition number grows exponentially as the trajectory length increases. The LSS problem produces solutions that gradually depend on s . As shown in Figure 3, it stays well-conditioned regardless of how long the trajectory is.

The LSS problem is well-conditioned a result not only observed in the Lorenz system, but also derives from

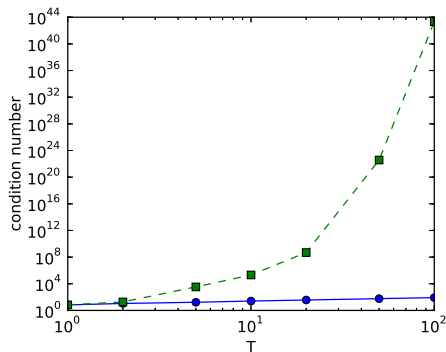


Figure 3: The condition number increases rapidly in an initial value problem (dashed line with squares), but stays relatively constant in an LSS problem (solid line with circles).

²In Figure 2(b), we solve a single initial value problem at $s = 25$, followed by a sequence of Least squares problems at increasing values of s , each using the previous solution as its reference trajectory u_r .

the *shadowing lemma*[21]. It guarantees that a trajectory of the governing equation exists in the proximity of any “ δ -pseudo trajectory”, defined as an approximate solution that satisfies the governing equation to δ -precision. The lemma assumes a set of properties known as *uniform hyperbolicity*[22, 23], and states that *for any $\epsilon > 0$, there exists δ , such that for all δ -pseudo trajectory u_r of any length, there exists a true trajectory u within ϵ distance from u_r , in the same distance metric used in Equation (10)*. If u_r is a true trajectory at input value s , and thereby a $\delta = \sup \frac{\partial f(u;s)}{\partial s} \delta s$ -pseudo-trajectory at input value $s + \delta s$, then the shadowing lemma predicts the LSS solution u_{lss} to be within ϵ distance from u_r . Perturbing s slightly makes u_{lss} slightly different from u_r , indicating a well-conditioned problem regardless of how long the trajectory is.

Because the LSS problem is well-conditioned, its time averaged output $\bar{J}_{lss}^{(T)}(s)$ has a useful derivative. This LSS derivative $\frac{d\bar{J}_{lss}^{(T)}}{ds}$ can be computed by solving a linearized LSS problem (detailed in Section 4.3). Because of its well-conditioning, perturbing the input between s and $s + \delta s$ causes a small difference in its solution, and therefore a small difference in the LSS derivative. This, and the fundamental theorem of calculus

$$\frac{1}{\delta s} \int_s^{s+\delta s} \frac{d\bar{J}_{lss}^{(T)}}{ds} ds = \frac{\bar{J}_{lss}^{(T)}(s + \delta s) - \bar{J}_{lss}^{(T)}(s)}{\delta s}, \quad (12)$$

make the LSS derivative at any $s \in [s, s + \delta s]$ a useful approximation to the slope.

As $T \rightarrow \infty$, this slope converges to the slope of the infinite time average $\bar{J}^{(\infty)}$, and the LSS derivative converges to the derivative of this infinite time average. Such derivative exists not only as a derivative of the limit (9) [24, 23], but also as a limit of the LSS derivative as $T \rightarrow \infty$. The limit and the derivative commute because the slope of $\bar{J}^{(\infty)}$ between s and $s + \delta s$ uniformly converges to its derivative as δs vanishes – a proven result made possible by the well-conditioned LSS problem [25].

4.3. Computing derivative from linearized Least Squares Shadowing (LSS) solution

The linearized LSS problem derives from the nonlinear problem (10). We choose a reference trajectory u_r that satisfies the governing equation at an input value s , then perturb s by an infinitesimal δs . By ignoring $O(\delta s^2)$ terms in Taylor expansions, we obtain

$$\begin{aligned} & \underset{\eta, v}{\text{minimize}} \quad \frac{1}{T} \int_0^T (\|v\|^2 + \alpha^2 \eta^2) dt, \quad \text{such that} \\ & \frac{dv}{dt} = \frac{\partial f}{\partial u} v + \frac{\partial f}{\partial s} + \eta f(u_r, s), \end{aligned} \quad (13)$$

where $v(t)$ and $\eta(t)$ are the solution of this linearized LSS problem. They relate to the solution of the nonlinear problem $\tau_{lss}^{(T)}$ and $u_{lss}^{(T)}$ via

$$v(t) = \frac{d}{ds} \left(u_{lss}^{(T)} \left(\tau_{lss}^{(T)}(t; s); s \right) \right), \quad \eta(t) = \frac{d}{ds} \frac{d\tau_{lss}^{(T)}(t; s)}{dt}. \quad (14)$$

The linearization is detailed in the Appendix. We also linearize the time averaged output $\bar{J}_{lss}^{(T)}$ as defined in Equation (11), and obtain a formula for computing the desired derivative from the solution of the linearized LSS problem

$$\frac{d\langle J \rangle}{ds} \approx \frac{\int_0^T \left(\frac{\partial J}{\partial u} v + \frac{\partial J}{\partial s} + \eta (J - \bar{J}) \right) dt}{T}, \quad \text{where } \bar{J} = \frac{\int_0^T J dt}{T} \quad (15)$$

This linearization is also derived in the Appendix.

5. Numerical solution of the Least Squares Shadowing (LSS) problem

The linearized LSS problem (13) can be solved with two numerical approaches. One approach, detailed in Subsection 5.1, first discretizes Problem (13), then derive from the discretized minimization problem its optimality condition, a system of linear equations that are finally solved to obtain the solution v and η . The other approach, detailed in Subsection 5.2, applies variational calculus to Problem (13) to derive its variational optimality condition, a system of linear differential equations that are then discretized and solved to obtain v and η . Both approaches can lead to the same linear system, whose solution method is described in Subsection 5.3. Section 5.4 provides a short summary of the numerical procedure. The algorithm admits an adjoint counterpart, described in Subsection 5.5, that can compute derivatives to many parameters simultaneously.

5.1. Derivation of the linear system via the discrete optimization approach

We first convert Problem (13) from a variational minimization problem to a finite dimensional minimization problem. By dividing the time domain $[0, T]$ into $m = T/\Delta t$ uniform time steps³, denoting $u_{i+\frac{1}{2}} = u_r \left(\left(i + \frac{1}{2} \right) \Delta t \right)$, $v_{i+\frac{1}{2}} = v \left(\left(i + \frac{1}{2} \right) \Delta t \right)$, $i = 0, \dots, m-1$ and $\eta_i = \eta(i\Delta t)$, $i = 1, \dots, m-1$, and approximating the time derivatives of u and v via the trapezoidal rule⁴, we discretize

³ Δt is chosen to be uniform for all time steps because it simplifies the notation. The algorithm can be extended to nonuniform Δt , as implemented in the `lssode` package[26].

⁴ We choose the trapezoidal rule because it is single-step and second-order accurate. Other time discretization can be used, though the resulting system will be either more complex or less accurate.

the linearized LSS problem (13) into

$$\begin{aligned} \text{minimize}_{v_i, \eta_i} \quad & \sum_{i=0}^{m-1} \frac{\|v_{i+\frac{1}{2}}\|_2^2}{2} + \alpha^2 \sum_{i=1}^{m-1} \frac{\eta_i^2}{2}, \quad \text{such that} \\ & E_i v_{i-\frac{1}{2}} + f_i \eta_i + G_i v_{i+\frac{1}{2}} = b_i, \quad 1 \leq i < m \end{aligned} \quad (16)$$

where

$$\begin{aligned} E_i &= -\frac{I}{\Delta t} - \frac{\partial f}{\partial u}(u_{i-\frac{1}{2}}, s), \\ f_i &= \frac{u_{i+\frac{1}{2}} - u_{i-\frac{1}{2}}}{\Delta t}, \\ G_i &= \frac{I}{\Delta t} - \frac{\partial f}{\partial u}(u_{i+\frac{1}{2}}, s). \\ b_i &= \frac{1}{2} \left(\frac{\partial f(u_{i-\frac{1}{2}}, s)}{\partial s} + \frac{\partial f(u_{i+\frac{1}{2}}, s)}{\partial s} \right), \end{aligned} \quad (17)$$

This linear-constrained least-squares problem has an optimality condition that forms the following KKT system[27]

$$\left[\begin{array}{cccccccc|cccc} I & & & & & & & & E_1^T & & & & & & v_{\frac{1}{2}} \\ & \alpha^2 & & & & & & & f_1^T & & & & & & \eta_1 \\ & & I & & & & & & G_1^T & E_2^T & & & & & v_{1+\frac{1}{2}} \\ & & & \alpha^2 & & & & & & f_2^T & & & & & \eta_2 \\ & & & & I & & & & & G_2^T & & & & & v_{2+\frac{1}{2}} \\ & & & & & \ddots & & & & & \ddots & & & & \vdots \\ & & & & & & \alpha^2 & & & & & E_{m-1}^T & & & 0 \\ & & & & & & & I & & & & f_{m-1}^T & & & \eta_{m-1} \\ & & & & & & & & & & & G_{m-1}^T & & & v_{m-\frac{1}{2}} \\ \hline E_1 & f_1 & G_1 & & & & & & & & & & & & w_1 \\ & & & E_2 & f_2 & G_2 & & & & & & & & & w_2 \\ & & & & & & \ddots & & & & & & & & \vdots \\ & & & & & & & & E_{m-1} & f_{m-1} & G_{m-1} & & & & w_{m-1} \end{array} \right] = \begin{bmatrix} 0 \\ 0 \\ 0 \\ 0 \\ 0 \\ \vdots \\ 0 \\ 0 \\ -b_1 \\ -b_2 \\ \vdots \\ -b_{m-1} \end{bmatrix} \quad (18)$$

This linear system can be solved to obtain the LSS solution v_i and η_i .

5.2. Derivation of the linear system via the continuous optimization approach

Problem (13) is constrained by a differential equation. Its optimality condition must be derived using calculus of variation. Denote $w(t)$ as the Lagrange multiplier function; the Lagrangian of Problem (13) is

$$\Lambda = \int_0^T \left(v^\top v + \alpha^2 \eta^2 + 2w^\top \left(\frac{dv}{dt} - \frac{\partial f}{\partial u} v - \frac{\partial f}{\partial s} - \eta f \right) \right) dt$$

The optimality condition requires a zero variation of Λ with respect to arbitrary δw , δv and $\delta \eta$. This condition, through integration by parts, transforms into the following differential equations and boundary conditions

$$\begin{cases} \frac{dv}{dt} - \frac{\partial f}{\partial u} v - \frac{\partial f}{\partial s} - \eta f = 0 \\ \frac{dw}{dt} + \frac{\partial f}{\partial u}^\top w - v = 0 \\ w(0) = w(T) = 0 \\ \alpha^2 \eta - w^\top f = 0. \end{cases}$$

These linear differential equations consistently discretize into the same linear system (18) derived in the last subsection.

5.3. Solution of the linear system

The KKT system (18) can be solved by using Gauss elimination to remove the lower-left block, forming the Schur complement

$$\mathbf{B}\mathbf{B}^T \mathbf{w} = \mathbf{b}, \quad (19)$$

where

$$\mathbf{B} = \begin{bmatrix} E_1 & \frac{f_1}{\alpha} & G_1 & & & \\ & E_2 & \frac{f_2}{\alpha} & G_2 & & \\ & & \ddots & \ddots & & \\ & & & E_m & \frac{f_m}{\alpha} & G_m \end{bmatrix}, \quad \mathbf{w} = \begin{bmatrix} w_1 \\ w_2 \\ \vdots \\ w_m \end{bmatrix}, \quad \mathbf{b} = \begin{bmatrix} b_1 \\ b_2 \\ \vdots \\ b_m \end{bmatrix}. \quad (20)$$

This Schur complement matrix $\mathbf{B}\mathbf{B}^T$ is symmetric-positive-definite and block-tri-diagonal; its block size is the dimension of the dynamical system n . Equation (19) can be solved using a banded direct solver with $O(mn^3)$ floating point operations [28]. One can also apply sparse QR factorization to the block-bi-diagonal \mathbf{B}^T , and then use backward and forward substitution to compute \mathbf{w} . The factorization also takes $O(mn^3)$ floating point operations [28]. Iterative methods can be used when n is large.

\mathbf{w} is substituted into the upper blocks of Equation (18) to compute v_i and η_i . These blocks can be written as

$$v_{i+\frac{1}{2}} = -G_i^T w_i - E_{i+1}^T w_{i+1}, \quad 0 \leq i < m; \quad \eta_i = -\frac{f_i^T w_i}{\alpha^2}, \quad 0 < i < m. \quad (21)$$

with the notation $w_0 = w_{m+1} = 0$. The desired derivative is then computed by discretizing Equation (15) into

$$\frac{d\langle J \rangle}{ds} \approx \frac{1}{m} \sum_{i=0}^{m-1} \left(\frac{\partial J(u_{i+\frac{1}{2}}, s)}{\partial u} v_{i+\frac{1}{2}} + \frac{\partial J(u_{i+\frac{1}{2}}, s)}{\partial s} \right) + \frac{1}{m-1} \sum_{i=1}^{m-1} \eta_i \tilde{J}_i \quad (22)$$

where

$$\tilde{J}_i = \frac{J(u_{i-\frac{1}{2}}, s) + J(u_{i+\frac{1}{2}}, s)}{2} - \frac{1}{m} \sum_{i=0}^{m-1} J(u_{i+\frac{1}{2}}, s), \quad i = 1, \dots, m-1 \quad (23)$$

5.4. Summary of the algorithm

1. Choose a small time step size Δt and sufficient number of time steps m .
2. Compute a solution to the equation (1) at $u_i = u_r((i + \frac{1}{2})\Delta t), i = 0, \dots, m - 1$.
3. Compute the vectors and matrices E_i, f_i, G_i and b_i as defined in Equations (17).
4. Form matrix \mathbf{B} . Choose an α so that f_i/α is on the same order of magnitude as E_i and G_i . Solve Equation (19) for \mathbf{w} .
5. Compute v_i and η_i from Equation (21).
6. Compute desired derivative using Equation (22).

The computational cost is $O(mn^3)$ if a direct solver is used for Equation (19), where m is the number of time steps and n is the dimension of the dynamical system.

5.5. Adjoint formulation of the sensitivity computation method

The discrete adjoint computes the same derivative as in Equation (22) by first solving the adjoint system

$$\left[\begin{array}{cccc|cccc}
 I & & & & E_1^T & & & \\
 & \alpha^2 & & & f_1^T & & & \\
 & & I & & G_1^T & E_2^T & & \\
 & & & \alpha^2 & & f_2^T & & \\
 & & & & & G_2^T & & \\
 & & & & & & \ddots & E_{m-1}^T \\
 & & & & & & & f_{m-1}^T \\
 & & & & & & & G_{m-1}^T \\
 \hline
 E_1 & f_1 & G_1 & & & & & \\
 & & E_2 & f_2 & G_2 & & & \\
 & & & & \ddots & \ddots & & \\
 & & & & & E_{m-1} & f_{m-1} & G_{m-1}
 \end{array} \right] \begin{bmatrix} \hat{v}_{\frac{1}{2}} \\ \hat{\eta}_1 \\ \hat{v}_{1+\frac{1}{2}} \\ \hat{\eta}_2 \\ \hat{v}_{2+\frac{1}{2}} \\ \vdots \\ \hat{\eta}_{m-1} \\ \hat{v}_{m-\frac{1}{2}} \\ \hat{w}_1 \\ \hat{w}_2 \\ \vdots \\ \hat{w}_{m-1} \end{bmatrix} = \begin{bmatrix} \frac{1}{m} \frac{\partial J(u_{1/2}, s)}{\partial u} \\ \frac{1}{m-1} \tilde{J}_1 \\ \frac{1}{m} \frac{\partial J(u_{1+1/2}, s)}{\partial u} \\ \frac{1}{m-1} \tilde{J}_2 \\ \frac{1}{m} \frac{\partial J(u_{2+1/2}, s)}{\partial u} \\ \vdots \\ \frac{1}{m-1} \tilde{J}_{m-1} \\ \frac{1}{m} \frac{\partial J(u_{m-1/2}, s)}{\partial u} \\ \hline 0 \\ 0 \\ \vdots \\ 0 \end{bmatrix} \quad (24)$$

The system has the same matrix as Equation (18), but a different right hand side. It can be solved by inverting

$$\mathbf{B}\mathbf{B}^T \hat{\mathbf{w}} = \mathbf{B}\mathbf{g}, \quad (25)$$

where \mathbf{B} is defined in Equation (20), $\hat{\mathbf{w}} = (\hat{w}_1, \dots, \hat{w}_{m-1})$, and \mathbf{g} is the upper part of Equation (24)'s right hand side. Once $\hat{\mathbf{w}}$ is computed, $d\langle J \rangle/ds$ can be computed via

$$\frac{d\langle J \rangle}{ds} \approx \sum_{i=1}^{m-1} b_i^T \hat{w}_i + \frac{1}{m} \sum_{i=0}^{m-1} \frac{\partial J(u_{i+\frac{1}{2}}, s)}{\partial s}, \quad (26)$$

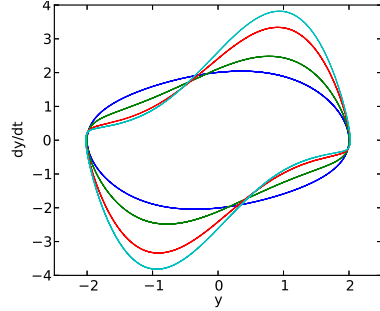
where b_i is defined in Equation (17). This adjoint derivative equals to the derivative computed in Section 5.4 up to round-off error. The examples in this paper use the algorithm in Section 5.4.

6. Application to the Van der Pol oscillator

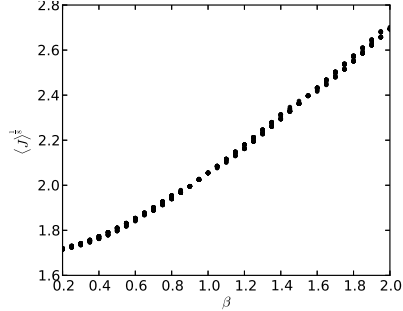
We apply our method to the Van der Pol oscillator

$$\frac{d^2y}{dt^2} = -y + \beta(1 - y^2)\frac{dy}{dt}. \quad (27)$$

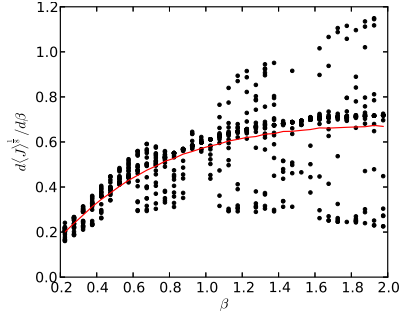
to compute sensitivity to the parameter β in the system. Figure 4a shows the



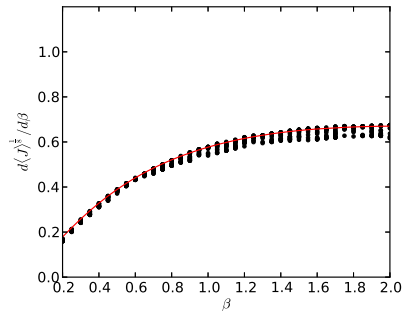
(a) Limit cycle attractors of the Van der Pol oscillator at $\beta = 0.2, 0.8, 1.6$ and 2.0 .



(b) For each value of β , $\langle J \rangle^{\frac{1}{8}}$ is estimated 20 times by solving initial value problems of length 50 with random initial conditions.



(c) $d\langle J \rangle^{\frac{1}{8}}/d\beta$ estimated by finite differencing pairs of trajectories with $\Delta\beta = 0.05$. For each value of β , the black dots are computed on 20 pairs of trajectories with length 50. The red line is computed on pairs of trajectories with length 5000.



(d) $d\langle J \rangle^{\frac{1}{8}}/d\beta$ estimated with Least Squares Shadowing sensitivity analysis. For each value of β , the black dots are computed on 20 trajectories of length 50. The red line is computed on trajectories of length 5000.

Figure 4: Least Squares Shadowing Sensitivity Analysis of the van der Pol oscillator.

limit cycle attractor as β varies from 0.2 to 2.0. As β increases, the maximum magnitude of dy/dt significantly increases. We choose the objective function to be the L^8 norm of dy/dt , which has a similar trend to the L^∞ norm and reflects the magnitude of the peak in dy/dt . By denoting $u = (u^{(1)}, u^{(2)}) = (y, dy/dt)$ as the state vector, we convert the second order ODE (27) into two coupled first

order ODEs, and write the objective function as

$$\langle J \rangle^{\frac{1}{8}} = \left(\lim_{T \rightarrow \infty} \frac{1}{T} \int_0^T J(u, \beta) dt \right)^{\frac{1}{8}}, \quad J(u, \beta) = \left(u^{(2)} \right)^8 \quad (28)$$

The method described in Section 4.3 is then applied to compute v : for each β , we start the simulation by assigning uniform $[0, 1]$ random numbers to $(u^{(1)}, u^{(2)})$ as their initial condition at $t = -50$. This initial time is chosen to be large enough so that when the ODE is integrated to $t = 0$, its state $u(0)$ is on its attractor. A trajectory $u(t), 0 \leq t \leq 50$ is then computed using a scipy[29] wrapper of lsoda[30], with time step size $\Delta t = 0.02$. The trajectory is about 50 times the longest timescale of the system. The $m = 2500$ states along the resulting trajectory are used to construct the coefficient in Equation (18).

The solution to Equation (18) is then substituted into Equation (22) to estimate the derivative of the $\langle J \rangle$ to the parameter β . Finally, the derivative of the output $\langle J \rangle^{\frac{1}{8}}$ is computed using

$$\frac{d\langle J \rangle^{\frac{1}{8}}}{d\beta} = \frac{\langle J \rangle^{-\frac{7}{8}} d\langle J \rangle}{8 d\beta}. \quad (29)$$

The computed derivative is compared against finite difference in Figure 4. For each value of β , we repeat both the finite difference and least squares shadowing 20 times on randomly initialized trajectories; the spread of the computed derivatives represents the approximation error due to insufficient trajectory length. Long trajectories are used to compute more accurate derivatives. The results indicate that the least squares shadowing method is more accurate than finite difference in this problem with the same trajectory length.

7. Application to the Lorenz system

We apply our method to the Lorenz system

$$\frac{dx}{dt} = \sigma(y - x), \quad \frac{dy}{dt} = x(r - z) - y, \quad \frac{dz}{dt} = xy - \beta z. \quad (30)$$

and analyze sensitivity to the parameter ρ in the system. The behavior of the Lorenz system as ρ changes from 0 to 100 is shown in Figure 5a, and can be summarized as following [31]:

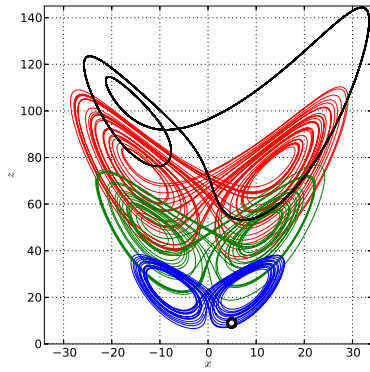
- Stable fixed point attractor at $(0, 0, 0)$ for $0 \leq \rho \leq 1$.
- Two stable fixed point attractors at $x = y = \pm \sqrt{\beta(\rho - 1)}, z = \rho - 1$ for $1 < \rho < 24.74$.
- Quasi-hyperbolic strange attractors for $24.06 < \rho < 31$. This includes the classic Lorenz attractor at $\rho = 28$.
- Non-hyperbolic quasi-attractors for $31 < \rho < 99.5$.

- Periodic limit cycle attractors with an infinite series of period doubling for $\rho > 99.5$.

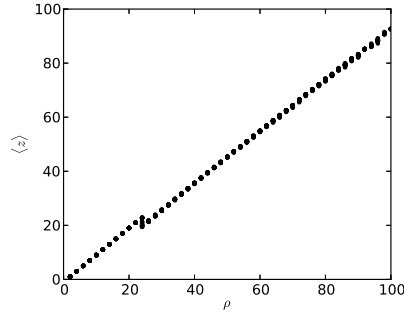
Despite the many transitions in the fundamental nature of the system, the mean z value

$$\langle z \rangle = \lim_{T \rightarrow \infty} \frac{1}{T} \int_0^T z dt \quad (31)$$

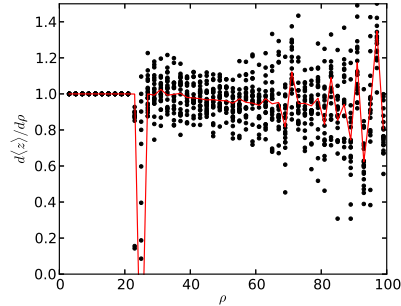
apparently increases as the parameter ρ increases. $\langle z \rangle$ is chosen to be our time averaged output quantity in this study.



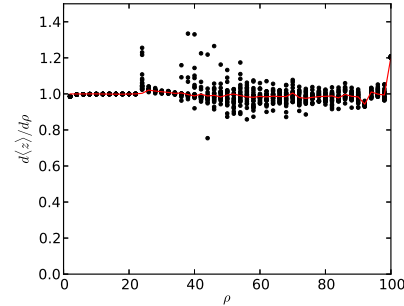
(a) Attractors of the Lorenz system at $\rho = 10$ (open circle), $\rho = 25, 50, 75$ and 100 (blue, green, red and black lines, respectively)



(b) For each value of ρ , $\langle z \rangle$ is estimated 20 times by solving initial value problems of length 50 with random initial conditions.



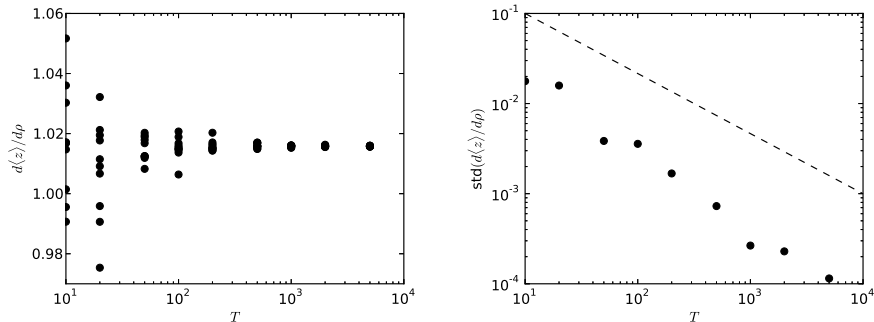
(c) $d\langle z \rangle/d\rho$ estimated by finite differencing pairs of trajectories with $\Delta\rho = 2$. For each value of ρ , the black dots are computed on 20 pairs of trajectories with length 50. The red line is computed on pairs of trajectories with length 5000.



(d) $d\langle z \rangle/d\rho$ estimated with Least Squares Shadowing sensitivity analysis. For each value of ρ , the black dots are computed on 20 trajectories of length 50. The red line is computed on trajectories of length 5000.

Figure 5: Least Squares Shadowing Sensitivity Analysis of the Lorenz system.

By denoting $u = (x, y, z)$, the method described in Section 5.4 is applied to the Lorenz system. For each ρ , we start the simulation at $t = -50$ with uniform $[0, 1]$ random numbers as initial conditions for x, y and z . The Lorenz system is integrated to $t = 0$, so that $u(0)$ is approximately on the attractor. A trajectory $u(t), 0 \leq t \leq 50$ is then computed using a `scipy`[29] wrapper of `lsoda`[30], with time step size $\Delta t = 0.01$. The resulting $m = 5000$ states along the trajectory are used to construct the linear system (18), whose solution is then used to estimate the desired derivative $d\langle z \rangle/d\rho$ using Equation (15).



(a) For each time length T , the Least squares shadowing algorithm runs on 10 random trajectories, computing 10 different derivatives.

(b) The sample standard deviation of the 10 derivatives at each trajectory length T .

Figure 6: Convergence of Least Squares Shadowing Sensitivity Analysis applied to the Lorenz system.

The computed derivative is compared against finite difference values in Figure 5. The dip in the finite difference value at around $\rho = 22.5$ is due to a bifurcation from fixed point attractors to strange attractors at $24.0 \leq \rho \leq 24.74$ (the two types of attractors co-exist within this range). For $24.74 < \rho < 31$, the Lorenz system is dominated by a quasi-hyperbolic attractor. Least squares shadowing sensitivity analysis computes accurate and consistent gradients on randomly chosen short trajectories on the attractor. The computed gradients has a random error on the order of $O(T^{-\frac{1}{2}})$, a result derived theoretically for discrete-time dynamical systems [25] and shown empirically here in Figure 6.

As ρ increases beyond 31, the system is non-hyperbolic and its trajectories form an object known as a quasi-attractor [32]. For $\rho > 99.5$, the system transitions to periodic oscillations, then goes through an infinite series of period doubling bifurcations. Despite of the complex, non-hyperbolic behavior, our method computes derivatives that are more accurate than finite difference on the same trajectory lengths.

8. Application to an aero-elastic limit cycle oscillator

We apply our method to a simple model of aeroelastic limit cycle oscillation, as shown in Figure 7. The model is described in detail by Zhao and Yang[33].

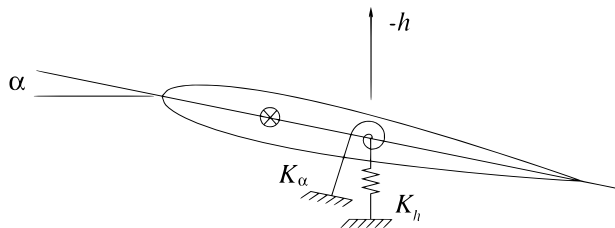


Figure 7: Model aero-elastic oscillator

The governing equations are

$$\begin{aligned} \frac{d^2 h}{dt^2} + 0.25 \frac{d\alpha}{dt} + 0.1 \frac{dh}{dt} + 0.2 h + 0.1 Q \alpha &= 0 \\ 0.25 \frac{d^2 h}{dt^2} + 0.5 \frac{d^2 \alpha}{dt^2} + 0.1 \frac{d\alpha}{dt} + 0.5 \alpha + 20 \alpha^3 - 0.1 Q \alpha &= 0 \end{aligned} \quad (32)$$

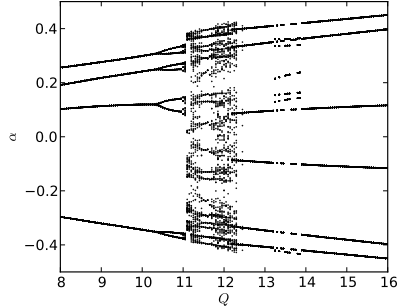
where h is the plunging degree of freedom, and α is the pitching degree of freedom. We analyze sensitivity to the reduced dynamic pressure Q .

The bifurcation diagram of α as Q increases from 8 to 16 is shown in Figure 8a. The behavior of the system as Q varies is complex [34]: At low values of Q , the system has an asymmetric limit cycle attractor. As Q increases beyond about 10.25, a series of period doubling bifurcations occurs, leading to transition into chaos just beyond $Q = 11$. At about $Q = 12.5$, the system ceases to be chaotic, and transitions to symmetric periodic limit cycle oscillation. When Q increases beyond about 13.25, there appears to be small windows of asymmetric oscillations. Finally, at about $Q = 13.9$, the system recovers symmetric periodic limit cycle oscillations. The phase plot of the system at several values of Q is shown in Figure 8b. These include an asymmetric periodic limit cycle attractor at $Q = 8$, a chaotic limit cycle attractor or quasi-attractor at $Q = 12$, and a symmetric periodic limit cycle attractor at $Q = 16$.

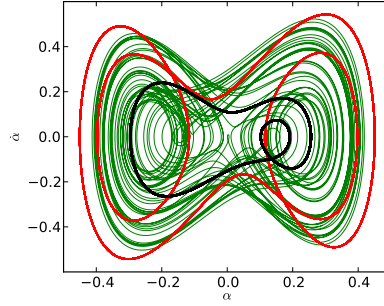
We observe that the magnitude of the oscillation grows as Q increases, and choose the L^8 norm of the pitch angle α as the objective function. The L^8 norm has similar trend as the L^∞ norm, and indicates the magnitude of the oscillation in the pitching degree of freedom. Denoting $u = (u^{(1)}, u^{(2)}, u^{(3)}, u^{(4)}) = (y, \alpha, dy/dt, d\alpha/dt)$ as the state vector, we convert the pair of second order ODEs (32) into a system of four first order ODEs. The output can then be written as

$$\langle J \rangle^{\frac{1}{8}} = \left(\lim_{T \rightarrow \infty} \frac{1}{T} \int_0^T u^{(2)8} dt \right)^{\frac{1}{8}} \quad (33)$$

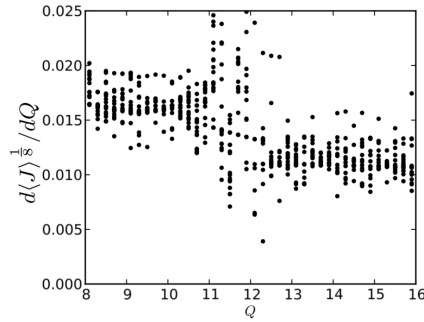
We use the method described in Section 5.4 to compute the derivative of the objective function to the input parameter Q . For each Q , we initiate the simulation at $t = -300$ with uniform $[0, 1]$ random numbers as its initial condition. The ODE is integrated to $t = 0$ to ensure that $u(0)$ is approximately on an attractor. A trajectory $u(t), 0 \leq t \leq 300$ is then computed using a scipy[29]



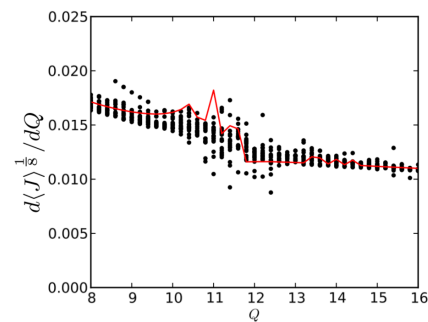
(a) Bifurcation diagram in the parameter range considered.



(b) Phase plots (α vs $\dot{\alpha} = d\alpha/dt$) at $Q = 8$ (black), $Q = 12$ (green) and $Q = 16$ (red).



(c) $d\langle J \rangle^{1/8} / dQ$ estimated by finite differencing pairs of trajectories with $\Delta Q = 0.2$. For each value of Q , the black dots are computed on 20 pairs of trajectories with length 300.



(d) $d\langle J \rangle^{1/8} / dQ$ estimated with Least Squares Shadowing sensitivity analysis. For each value of Q , the black dots are computed on 20 trajectories of length 300. The red line is computed on trajectories of length 30000.

Figure 8: Least Squares Shadowing Sensitivity Analysis on the aero-elastic oscillator model (32).

wrapper of `lsoda`[30], with time step size $\Delta t = 0.02$. The resulting 15000 states along the trajectory are used to construct the linear system (18), whose solution is used to estimate the derivative of the output with respect to Q . The computed derivative is compared against finite difference values in Figure 8. Whether the system exhibits periodic or chaotic limit cycle oscillations, the derivative computed using least squares shadowing sensitivity analysis is more accurate than finite difference results.

9. Conclusion

We presented the Least Squares Shadowing method for computing derivatives in ergodic dynamical systems. Traditional tangent and adjoint meth-

ods linearize the ill-conditioned initial value problem, thereby computing large derivatives useless for control, optimization and inference problems. The new method linearizes the well-conditioned least squares shadowing problem, thereby computing useful derivatives of long time averaged quantities. The method is demonstrated on the periodic van der Pol oscillator, the chaotic Lorenz attractor, and a simple aero-elastic oscillation model that exhibits mixed periodic and chaotic behavior. These applications demonstrate the effectiveness of our new sensitivity computation algorithm in many complex nonlinear dynamics regimes. These include fixed points, limit cycles, quasi-hyperbolic and non-hyperbolic strange attractors.

The Least Squares Shadowing method requires solving either a sparse matrix system (in its discrete formulation) or a boundary value problem in time (in its continuous formulation). This boundary value problem is about twice as large as a linearized initial value problem, in terms of the dimension and sparsity of the matrix for the discrete formulation, and in terms of the number of equations for the continuous formulation. When the dynamical system is low dimensional, the sparse matrix system can be solved using a direct matrix solver; computing the derivative of the output costs a few times more than computing the output itself by solving an initial value problem. When the dynamical system is high dimensional, e.g., a discretized partial differential equation, iterative solution methods should be used instead of direct matrix solvers. Because the system is well-conditioned and only twice as large as an initial value problem, an iterative solution can potentially cost only a small multiple of an initial value solution, particularly if using an iterative solver specifically designed for this problem. Therefore, we think that the Least Squares Shadowing method is not only efficient for low-dimensional chaotic dynamical systems, but also applicable to sensitivity analysis of large chaotic dynamical systems.

Acknowledgments

The first author acknowledges AFOSR Award F11B-T06-0007 under Dr. Fariba Fahroo, NASA Award NNH11ZEA001N under Dr. Harold Atkins, and a subcontract of the DOE PSAAP Program at Stanford.

References

- [1] Jameson, A., “Aerodynamic Design via Control Theory,” *Journal of Scientific Computing*, Vol. 3, 1988, pp. 233–260.
- [2] Reuther, J., Jameson, A., Alonso, J., Rimlinger, M., and Saunders, D., “Constrained multipoint aerodynamic shape optimization using an adjoint formulation and parallel computers,” *Journal of aircraft*, Vol. 36, No. 1, 1999, pp. 51–60.
- [3] Bewley, T., “Flow control: new challenges for a new Renaissance,” *Progress in Aerospace Sciences*, Vol. 37, No. 1, 2001, pp. 21–58.

- [4] Bewley, T., Moin, P., and Temam, R., “DNS-based predictive control of turbulence: an optimal target for feedback algorithms,” *J. Fluid Mech.*, Vol. 447, 2001, pp. 179–225.
- [5] Tromp, J., Tape, C., and Liu, Q., “Seismic tomography, adjoint methods, time reversal and banana-doughnut kernels,” *Geophysical Journal International*, Vol. 160, No. 1, 2005, pp. 195–216.
- [6] Becker, R. and Rannacher, R., “An optimal control approach to a posteriori error estimation in finite element methods,” *Acta Numerica*, Cambridge University Press, 2001.
- [7] Giles, M. and Suli, E., “Adjoint methods for PDEs: a posteriori error analysis and postprocessing by duality,” *Acta Numer.*, Vol. 11, 2002, pp. 145–236.
- [8] Hartmann, R., Held, J., Leicht, T., and Prill, F., “Error Estimation and Adaptive Mesh Refinement for Aerodynamic Flows,” *ADIGMA - A European Initiative on the Development of Adaptive Higher-Order Variational Methods for Aerospace Applications*, edited by N. Kroll, H. Bieler, H. Deconinck, V. Couaillier, H. Ven, and K. Srensen, Vol. 113 of *Notes on Numerical Fluid Mechanics and Multidisciplinary Design*, Springer Berlin Heidelberg, 2010, pp. 339–353.
- [9] Fidkowski, K. J. and Darmofal, D. L., “Review of output-based error estimation and mesh adaptation in computational fluid dynamics,” *AIAA journal*, Vol. 49, No. 4, 2011, pp. 673–694.
- [10] Thepaut, J.-N. and Courtier, P., “Four-dimensional variational data assimilation using the adjoint of a multilevel primitive-equation model,” *Quarterly Journal of the Royal Meteorological Society*, Vol. 117, No. 502, 1991, pp. 1225–1254.
- [11] Courtier, P., Derber, J., Errico, R., Louis, J. F., and Vukicevic, T., “Important literature on the use of adjoint, variational methods and the Kalman filter in meteorology,” *Tellus A*, Vol. 45, No. 5, 2002, pp. 342–357.
- [12] Wang, Q., *Uncertainty Quantification for Unsteady Fluid Flow using Adjoint-based Approaches*, Ph.D. thesis, Stanford University, Stanford, CA, 2009.
- [13] Lea, D., Allen, M., and Haine, T., “Sensitivity analysis of the climate of a chaotic system,” *Tellus*, Vol. 52A, 2000, pp. 523–532.
- [14] Eyink, G., Haine, T., and Lea, D., “Ruelle’s linear response formula, ensemble adjoint schemes and Lévy flights,” *Nonlinearity*, Vol. 17, 2004, pp. 1867–1889.

- [15] Thuburn, J., “Climate sensitivities via a Fokker-Planck adjoint approach,” *Quarterly Journal of the Royal Meteorological Society*, Vol. 131, No. 605, 2005, pp. 73–92.
- [16] Abramov, R. and Majda, A., “Blended response algorithms for linear fluctuation-dissipation for complex nonlinear dynamical systems,” *Nonlinearity*, Vol. 20, No. 12, 2007, pp. 2793.
- [17] Cooper, F. and Haynes, P., “Climate Sensitivity via a Nonparametric Fluctuation-Dissipation Theorem,” *Journal of the Atmospheric Sciences*, Vol. 68, No. 5, 2011, pp. 937–953.
- [18] Wang, Q., “Forward and Adjoint Sensitivity Computation for Chaotic Dynamical Systems,” *Journal of Computational Physics*, Vol. 235, No. 15, 2013, pp. 1–15.
- [19] Bryson, A. and Ho, Y., *Applied Optimal Control: Optimization, Estimation, and Control*, John Wiley & Sons Inc, Hoboken, NJ, 1979.
- [20] Wang, Q. and Gao, J., “The drag-adjoint field of a circular cylinder wake at Reynolds numbers 20, 100 and 500,” *Journal of Fluid Mechanics*, Vol. 730, 2013.
- [21] Pilyugin, S., *Shadowing in dynamical systems*, Vol. 1706, Springer, 1999.
- [22] Kuznetsov, S., *Hyperbolic Chaos: A Physicist’s View*, Springer Berlin Heidelberg, 2012.
- [23] Ruelle, D., “Differentiation of SRB states for hyperbolic flows,” *Ergodic Theory and Dynamical Systems*, Vol. 28, No. 02, 2008, pp. 613–631.
- [24] Ruelle, D., “Differentiation of SRB States,” *Communications in Mathematical Physics*, Vol. 187, 1997, pp. 227–241.
- [25] Wang, Q., “Convergence of the Least Squares Shadowing Method for Computing Derivative of Ergodic Averages,” *accepted for publication in SIAM J. Num. Anal.*, 2013, preprint available at arXiv:1304.3635.
- [26] Wang, Q., “The LSSODE Python module,” <https://github.com/qiqi/lssode>, 2013.
- [27] Boyd, S. P. and Vandenberghe, L., *Convex optimization*, Cambridge university press, 2004.
- [28] Golub, G. H. and Loan, C. F. V., *Matrix Computations*, The Johns Hopkins Univ. Press, Baltimore, 1996.
- [29] Jones, E., Oliphant, T., Peterson, P., et al., “SciPy: Open source scientific tools for Python,” 2001–2013, <http://www.scipy.org/>.

- [30] Petzold, L., “Automatic Selection of Methods for Solving Stiff and Nonstiff Systems of Ordinary Differential Equations,” *SIAM Journal on Scientific and Statistical Computing*, Vol. 4, No. 1, 1983, pp. 136–148.
- [31] Sparrow, C., *The Lorenz Equations: Bifurcations, Chaos, and Strange Attractors*, Springer-Verlag, New York, 1982.
- [32] Bonatti, C., Díaz, L., and Viana, M., *Dynamics Beyond Uniform Hyperbolicity: A Global Geometric and Probabilistic Perspective*, Encyclopaedia of Mathematical Sciences, Springer, 2010.
- [33] Zhao, L. and Yang, Z., “Chaotic motions of an airfoil with non-linear stiffness in incompressible flow,” *Journal of Sound and Vibration*, Vol. 138, No. 2, 1990, pp. 245–254.
- [34] Lee, B., Price, S., and Wong, Y., “Nonlinear aeroelastic analysis of airfoils: bifurcation and chaos,” *Progress in Aerospace Sciences*, Vol. 35, No. 3, 1999, pp. 205–334.

Appendix A. Derivation of Equations (13) and (15)

If $\frac{du_r}{dt} = f(u_r, s)$ in Problem (10), then $u_{lss}(t; s) \equiv u_r(t)$ and $\tau_{lss}(t; s) \equiv t$ solve the problem. Because Problem (10) is well-conditioned, its solution at a perturbed parameter value $s + \delta s$ for the same u_r should be slightly different. Denote

$$v(t) := \frac{d}{ds} \left(u_{lss}(\tau_{lss}(t; s); s) - u_r(t) \right), \quad \eta(t) := \frac{d}{ds} \left(\frac{d\tau_{lss}(t; s)}{dt} - 1 \right), \quad (\text{A.1})$$

which for infinitesimal δs translate into

$$\begin{aligned} \tau_{lss}(t; s + \delta s) &= \int_0^t (1 + \eta(t')\delta s) dt', \\ u_{lss}(\tau_{lss}(t; s + \delta s); s + \delta s) &= u_r(t) + v(t)\delta s. \end{aligned} \quad (\text{A.2})$$

The second equation translates the objective function in Problem (10) into the objective function in Problem (13). $du_{lss}(t; s + \delta s)$ must satisfy the constraint

in Problem (10), which translates into (ignoring $O(\delta s^2)$ terms)

$$\begin{aligned}
& \frac{d}{dt}(u_r(t) + v(t)\delta s) \\
&= \frac{du_{lss}(\tau_{lss}(t; s + \delta s); s + \delta s)}{dt} \\
&= \frac{d\tau_{lss}(t; s + \delta s)}{dt} \frac{du_{lss}(\tau; s + \delta s)}{d\tau} \Big|_{\tau=\tau_{lss}(t; s + \delta s)} \\
&= \frac{d\tau_{lss}(t; s + \delta s)}{dt} f(u_{lss}(\tau_{lss}(t; s + \delta s); s + \delta s), s + \delta s) \\
&= (1 + \eta(t)\delta s) \left(f(u_r(t), s) + \frac{\partial f}{\partial u} v(t)\delta s + \frac{\partial f}{\partial s} \delta s \right) \\
&= f(u_r(t), s) + \eta(t)f(u_r(t), s)\delta s + \frac{\partial f}{\partial u} v(t)\delta s + \frac{\partial f}{\partial s} \delta s
\end{aligned} \tag{A.3}$$

Because $\frac{du_r}{dt} = f(u_r, s)$, we cancel all $O(1)$ terms, leaving only

$$\frac{dv}{dt} = \eta(t)f(u_r(t), s) + \frac{\partial f}{\partial u} v(t) + \frac{\partial f}{\partial s}, \tag{A.4}$$

the constraint in the linearized least squares shadowing problem (13).

For infinitesimal δs , the definition of $\bar{J}_{lss}^{(T)}(s)$ in Equation (11) leads to

$$\begin{aligned}
& \bar{J}_{lss}^{(T)}(s + \delta s) - \bar{J}_{lss}^{(T)}(s) \\
&= \frac{\int_{\tau(0; s + \delta s)}^{\tau(T; s + \delta s)} J(u_{lss}(t; s + \delta s), s + \delta s) dt}{\tau(T; s + \delta s) - \tau(0; s + \delta s)} - \frac{\int_{\tau(0; s)}^{\tau(T; s)} J(u_{lss}(t; s), s) dt}{\tau(T; s) - \tau(0; s)} \\
&= \frac{\int_0^T J(u_{lss}(\tau_{lss}(t; s + \delta s), s + \delta s), s + \delta s) \frac{d\tau(s; s + \delta s)}{dt} dt}{\tau(T; s + \delta s) - \tau(0; s + \delta s)} - \frac{\int_0^T J(u_r(t), s) dt}{\tau(T; s) - \tau(0; s)} \\
&= \frac{\int_0^T J(u_{lss}(\tau_{lss}(t; s + \delta s), s + \delta s), s + \delta s) \frac{d\tau(s; s + \delta s)}{dt} dt}{\int_0^T (1 + \eta(t')\delta s) dt'} - \frac{\int_0^T J(u_r(t), s) dt}{\int_0^T (1 + \eta(t')\delta s) dt'} \\
&+ \frac{\int_0^T J(u_r(t), s) dt}{\int_0^T (1 + \eta(t')\delta s) dt'} - \frac{\int_0^T J(u_r(t), s) dt}{T} \\
&= \frac{\int_0^T \left(\left(J(u_r(t), s) + \frac{\partial J}{\partial u} v(t) \delta s + \frac{\partial J}{\partial s} \delta s \right) (1 + \eta(t)) - J(u_r(t), s) \right) dt}{\int_0^T (1 + \eta(t')\delta s) dt'} \\
&+ \left(\int_0^T J(u_r(t), s) dt \right) \frac{- \int_0^T \eta(t')\delta s dt'}{T \int_0^T (1 + \eta(t')\delta s) dt'} \\
&= \left(\frac{\int_0^T \left(\frac{\partial J}{\partial u} v(t) + \frac{\partial J}{\partial s} + \eta(t) J(u_r(t), s) \right) dt}{\int_0^T (1 + \eta(t')\delta s) dt'} \right. \\
&\quad \left. - \frac{\left(\int_0^T J(u_r(t), s) dt \right) \left(\int_0^T \eta(t') dt' \right)}{T^2} \right) \delta s + O(\delta s^2) \\
&= \frac{\delta s}{T} \int_0^T \left(\frac{\partial J}{\partial u} v(t) + \frac{\partial J}{\partial s} + \eta(t) \left(J(u_r(t), s) - \bar{J}_{lss}^{(T)} \right) \right) dt + O(\delta s^2)
\end{aligned} \tag{A.5}$$

Therefore,

$$\begin{aligned}
\frac{d\bar{J}_{lss}^{(T)}}{ds} &= \lim_{\delta s \rightarrow 0} \frac{\bar{J}_{lss}^{(T)}(s + \delta s) - \bar{J}_{lss}^{(T)}(s)}{\delta s} \\
&= \frac{1}{T} \int_0^T \left(\frac{\partial J}{\partial u} v(t) + \frac{\partial J}{\partial s} + \eta(t) \left(J(u_r(t), s) - \bar{J}_{lss}^{(T)} \right) \right) dt
\end{aligned} \tag{A.6}$$